SolarPACES 2024, 30th International Conference on Concentrating Solar Power, Thermal, and Chemical Energy Systems

Measurement Systems, Devices, and Procedures

https://doi.org/10.52825/solarpaces.v3i.2356

@ Authors. This work is licensed under a Creative Commons Attribution 4.0 International License

Published: 25 Nov. 2025

High-Resolution Flux Measurement for High-Flux Solar Simulators

Characterisation of Irradiance Distribution with a Thermopile

Richard Felsberger^{1,*}, Armin Buchroithner¹, Bernhard Gerl², and Hannes Wegleiter¹

¹Institute of Electrical Measurement and Sensor Systems, University of Technology, Graz, Austria ²Research Group for Aircraft Systems, University of Technology, Vienna, Austria *Correspondence: Richard Felsberger, richard.felsberger@tugraz.at

Abstract. Concentrated solar power (CSP) systems impose high demands on individual components such as receivers, optical elements, etc due to high solar flux. Characterisation of these components often requires measurements under defined, constant conditions, which can be challenging or even be impossible in real-world applications due to changes in irradiance, weather conditions, accessibility, tracking inaccuracies, etc. Solar simulators are used for this purpose, with the challenge of providing sun-like, uniformly distributed and highly concentrated light. This paper presents an approach to automatically investigate the irradiance distribution of concentrated light in a solar simulator. A water-cooled flux meter (thermopile) is used in combination with an XY table to scan the area of interest, resulting in a high-resolution image of the irradiance distribution in the target area. The results are presented and discussed based on measurement data recorded in a real solar simulator. Issues such as sensor area i.e. spatial resolution, light spectrum dependence, temperature influence, and measurement speed are addressed.

Keywords: Flux Gauge, Thermopile, High-Flux Solar Simulators, Characterization, Concentrated Solar Power

1. Introduction

Solar simulators are widely used to empirically investigate CSP components under defined conditions. For this purpose, a wide range of solar simulators can be found, offering solar concentration factors from as low as 1 sun to more than 10 000 suns [1]. To accurately determine the irradiance in the target plane, cameras are frequently employed, sometimes in conjunction with a thermopile (fixed at a single point) or ray trace simulations, to estimate the flux distribution. These camera-based measurements (or simulations) are based on assumptions such as spark length of the light source, reflectivity, wavelength properties, temperature dependencies, etc. and are therefore subject to uncertainty. This paper describes a approach that eliminates most of these uncertainties by directly measuring the irradiance distribution using a thermopile and an XY table. Thus, the uncertainty depends solely on the accuracy of the thermopile sensor. [1], [2]

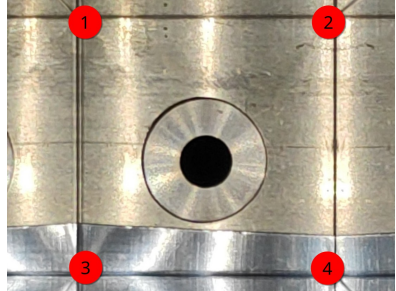


Figure 1. Photograph of the solar simulator during measurement. The four metal halide lamps and (elliptically shaped) reflector assembly (left) focus the light into the light guiding tunnel (LGT, centre right). On the opposite side of the tunnel (right) is a thermopile flux sensor mounted on an XY table, moving the sensor to measure the irradiance distribution.

2. Experimental Setups and Methodology

A custom-built solar simulator [3] is employed to demonstrate the operating principle of the measurement system. This solar simulator can generate irradiance levels from 1 to over 400 suns (i.e., $1\,\mathrm{kW\,m^{-2}}$ to $>\!400\,\mathrm{kW\,m^{-2}}$) and can be operated with or without a "Light Guiding Tunnel" (LGT). The LGT homogenizes the irradiance distribution, transforming a Gaussian peak into a more uniform, "flat" distribution [3]. This setup allows for the demonstration of the sensor principle with both, a typical Gaussian and an uniform light distributions. However, this paper focuses primarily on measurements taken with the LGT, as the significant radiation variations at the tunnel edges are particularly relevant to demonstrate the measurement principle. Figure 1 shows a photograph of the solar simulator. On the left, it depicts the four metal halide lamps with a total electrical power consumption of 4.8 kW. The light is focused into the LGT that directs/reflects the light toward the target area, where the flux sensor (thermopile) is mounted on the XY table. A polished aluminum tunnel is used as the LGT in this example (length $400 \, \mathrm{mm}$, aperture $50 \times 50 \,\mathrm{mm}^2$, distance between tunnel end and thermopile $5 \,\mathrm{mm}$). Depending on the desired light spectrum, alternative materials with different reflective properties could be used to adjust the spectrum sent to the target area. However, this aspect is not critical for the analyses presented in this paper, as the thermopile can measure radiation almost independently of the spectral distribution [2, pp. 6–7]. The thermopile is a calibrated, water-cooled Hukseflux SBG01-200. The irradiance is determined using Equation 1. where U represents the voltage in V, S is the sensitivity in $VW^{-1}m^2$ specified by the manufacturer in the calibration protocol (in this case, $(0.115 \pm 0.008) \times 10^{-6}$, k=2), and Φ is the irradiance in W m⁻². A Keithley 2100 digital multimeter (range: $100 \,\mathrm{mV}$, slow 6.5 digits) was used to systematically measure the thermopile voltage. The XY table was a Proxxon KT 70/CNC-ready with a resolution of 2.5 µm. The actively cooled room maintained a temperature of $\approx 21 \,^{\circ}\text{C}$.





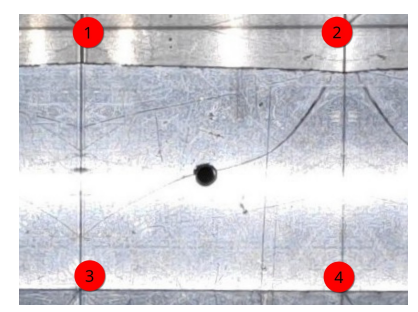


Figure 2. (Left) Entrance of the LGT at the focal point of the solar simulator, with the LGT exit directed towards the flux sensor. (Center) Uncovered flux sensor at the end of the LGT, with a sensor diameter of $10 \, \mathrm{mm}$ (black area). (Right) Partially covered flux sensor at the end of the LGT, with a sensor diameter of $3.15 \, \mathrm{mm}$ (black area). The red markers indicate the positions of the light guiding tunnel corners: 1 top left, 2 top right, 3 bottom left, 4 bottom right.

$$\Phi = \frac{U}{S} \tag{1}$$

A closer view of the LGT and the thermopile, which is surrounded by a water-cooled heat shield and mounted on the XY table, is shown in Figure 2 (left). Depending on the desired resolution, the XY table moves the thermopile across the target area, producing the previously described voltage signal and allows to (consequently) map the irradiance distribution. A simplified representation of this path is shown in Figure 3 (left). In this process, the XY table moves by the desired resolution, waits for $100\,\mathrm{ms}$, and then starts the measurement with the voltmeter. After the measurement is completed, the XY table moves to the next measurement point.

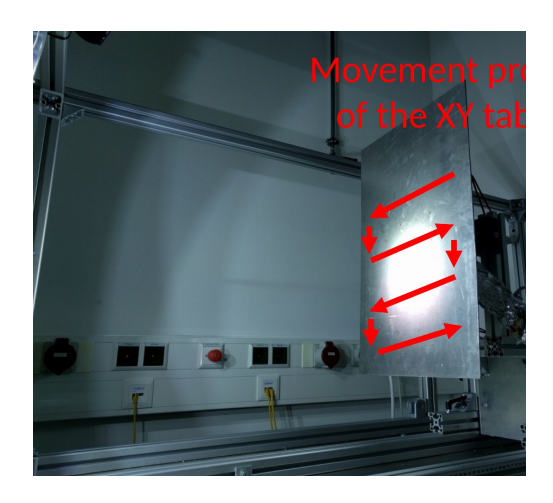
As shown in Figure 2 (center), the thermopile has a round black sensing area with a diameter of $10\,\mathrm{mm}$. This implies that the output signal from the thermopile represents the average of the radiation incident on that surface. To investigate the effects of this averaging, an additional aperture (heat shield) with a $3.15\,\mathrm{mm}$ diameter hole was manufactured and fitted to the measurement device (see Figure 2 (right)). This modification increases the spatial resolution of the sensor, although the sensitivity of the calibration may no longer be applicable and leads to incorrect (lower) irradiance results.

3. Results

This chapter is divided into three sections. The first section presents the results of measurements taken directly at the focal point of the elliptical reflectors. In this point, the focal points of all four compounds coincide due to the precise adjustments of the solar simulator (without the LGT). The second section addresses the measurements conducted using the LGT with different apertures for the thermopile. The third section addresses the time response of the thermopile and its impact on the measurements.

3.1 Focal Point

Figure 3 (left) shows a modified solar simulator setup. The LGT has been removed, and the thermopile sensor with the XY table has been positioned at the focal point of the four lamps. Additionally, a larger water-cooled heat cover was employed for improved radiation shielding. To ensure that the maximum allowable irradiance of the thermopile, which is $300\,\mathrm{suns}$, was not exceeded, the lamps were operated at $50\,\%$ power. The results of the measurement with an XY table resolution of $5\,\mathrm{mm}$ are presented in Figure 3 (right).



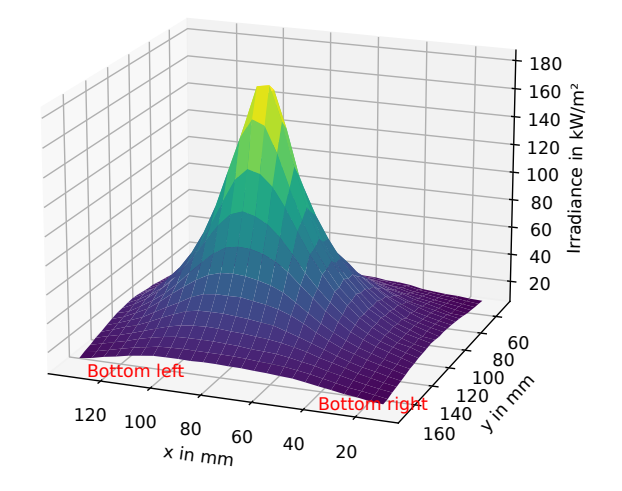


Figure 3. (Left) Solar simulator during measurement with the thermopile positioned at the focal point. (Right) Result of the irradiance distribution at the focal point. The Gaussian-like irradiance distribution is clearly visible. (Left) Modified from [3].

This measurement reveals a Gaussian-like radiation distribution with a peak irradiance of $\approx 180 \, \mathrm{suns}$.

3.2 Light Guiding Tunnel

The results of the irradiance distribution measurements using the LGT are discussed in this section (see Figure 1 and Figure 2 (left)). Initially, two measurements were conducted with the uncovered sensor (see Figure 2 (center)). One measurement was conducted covering the entire area of the tunnel exit at a lower resolution, while the second focused on one corner of the LGT with higher resolution (see Figure 4). The high-resolution measurement was performed only on one corner of the LGT to reduce the measurement time, a topic that will be addressed in more detail in a subsequent section. However, the results with the LGT clearly demonstrate the desired effect, namely a uniform radiation distribution over an area of $50 \times 50 \,\mathrm{mm}^2$. Irradiance values between 100 to 120 suns are observed at the edge of the plateau, and \approx 110 suns in the center. This is followed by a rapid decline at the edges of the LGT within $\approx 6 \, \mathrm{mm}$, dropping to almost 0 suns. A negative overshoot occurs when the black sensor area is no longer illuminated, but parts of the stainless steel housing surrounding the sensor area are (see Figure 2 (center)). This effect appears to be static rather than related to a transient response, as it is observed both when the thermopile is moved into and out of the illuminated area. A possible explanation is, that despite the water cooling of the thermopile sensor, the steel housing heats up due to incident radiation. This heat, transferred through good thermal contact, causes the back side of the thermopile to warm up while the front black side remains shaded and cooler, resulting in a negative voltage signal. This overshoot effect did not occur in subsequent measurements with a smaller aperture area and the shielded stainless steel housing of the thermopile sensor. The results of the high-resolution measurement (see Figure 4 (right)) reveal a similar but smoother curve, in addition to a higher density of data points. Notable in all measurements with the LGT is an oscillatory pattern observed on the right side of the tunnel edge (between the bottom right and top right). This pattern is also present on the opposite side (not visible), but not on the upper and lower edges. This effect can be attributed to the thermal inertia (i.e., transient response) of the sensor. As the XY table continuously moves out of the illuminated area and then back in after measuring the virtually unilluminated outer regions, large radiation gradients occur. Conversely, due to the path of the XY table, the

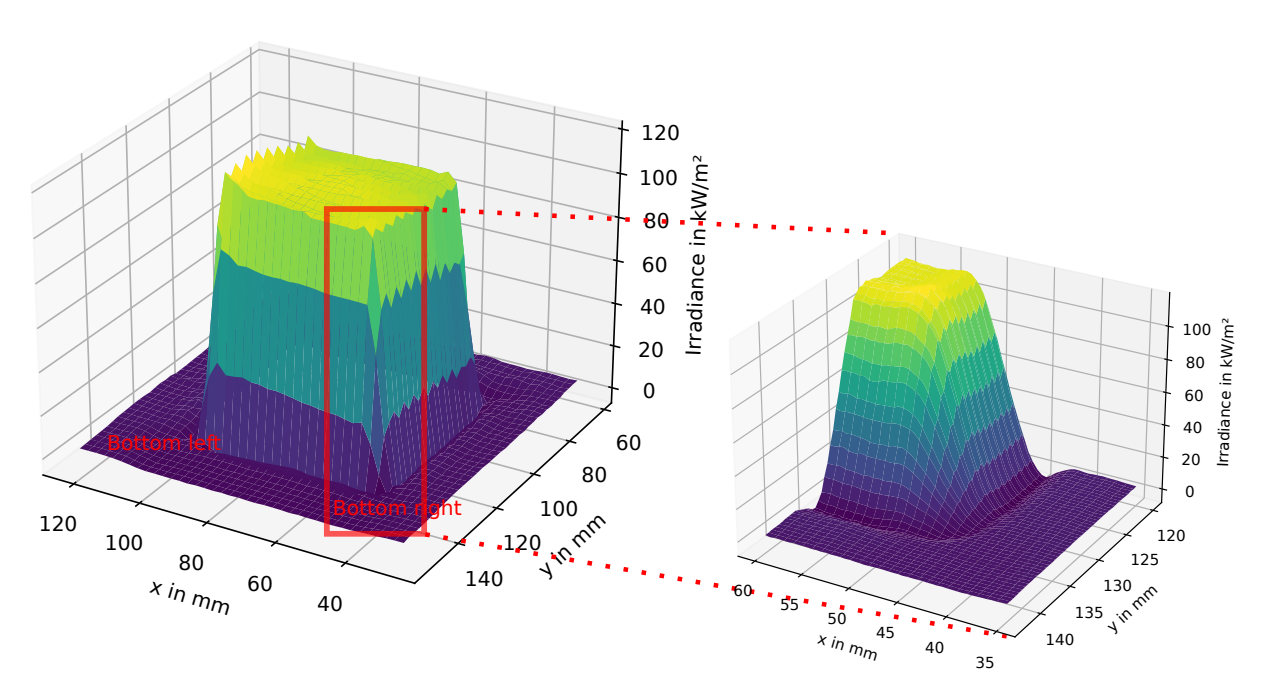


Figure 4. (Left) Measured irradiance distribution using the **uncovered** sensor, with a resolution of $2.5 \, \mathrm{mm}$. (Right) Measurement with higher resolution $(0.5 \, \mathrm{mm})$ focusing on the lower right corner of the LGT (viewed from the lamps towards the sensor).

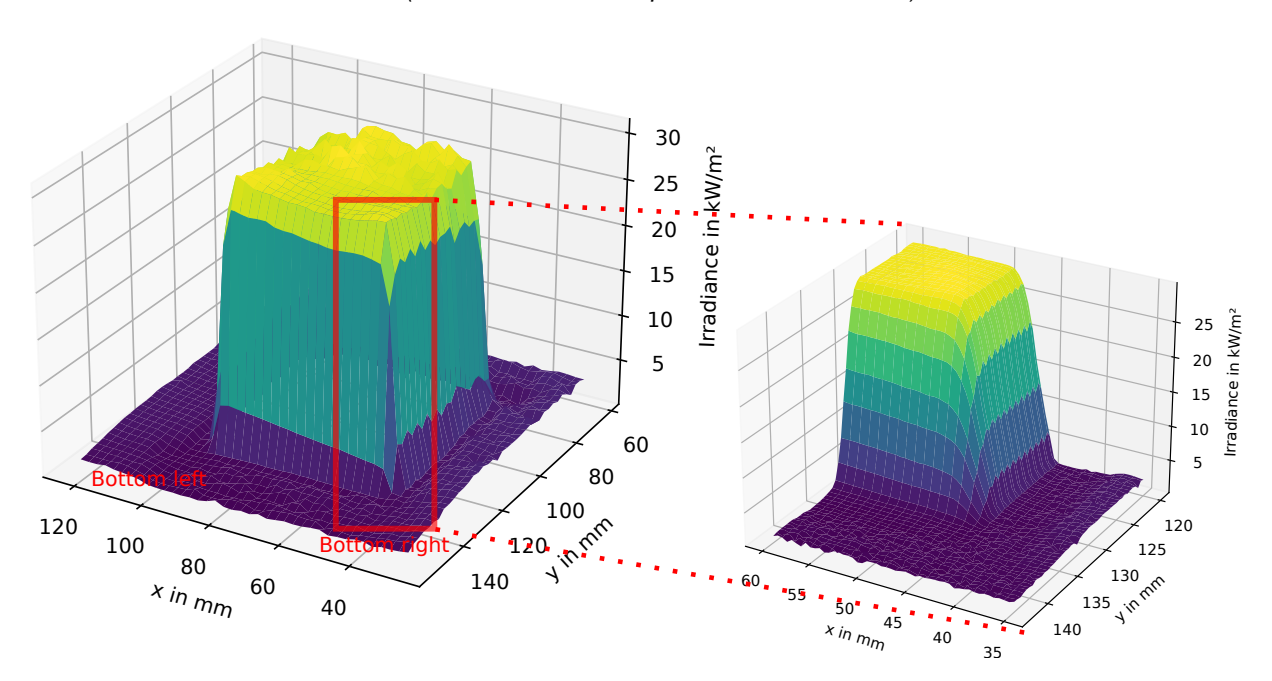


Figure 5. (Left) Measured irradiance distribution using the **covered** sensor, with a resolution of $2.5 \,\mathrm{mm}$. (Right) Measurement with higher resolution $(0.5 \,\mathrm{mm})$ focusing on the lower right corner of the LGT (viewed from the lamps towards the sensor). Note: The sensor is not recalibrated. The absolute values of the irradiance is not correct due to the partial shading of the sensor.

radiation remains almost constant when measuring the upper and lower edges. This issue can be mitigated by increasing the waiting time at each point until the sensor signal has fully stabilized, although this will significantly extend the measurement time (see next section). Alternatively, although not ideal, a rectangular path corresponding to the tunnel size can be traced, progressively reducing in size until reaching the center, instead of moving the XY table between the left and right edges. This approach would help to reduce the error associated with the transient response, as high radiation gradients can

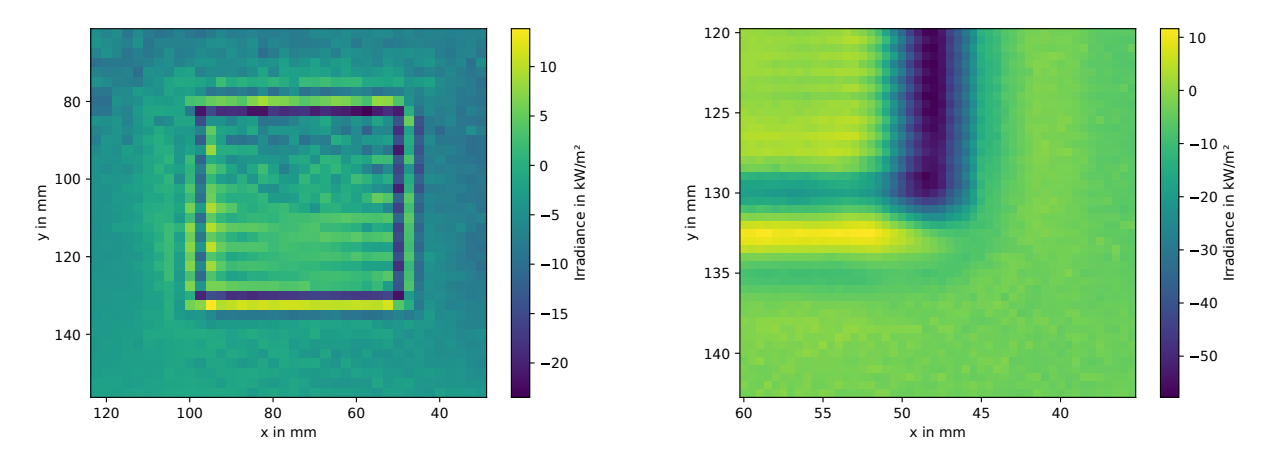


Figure 6. Difference between the results of the covered and uncovered flux sensor. (Left) Entire target plane measurement with lower resolution. (Right) Lower right corner with higher resolution. Results from the covered sensor are multiplied by 3.75 to compensate for the irradiance level.

be minimized, but require precise and time-consuming adjustments to the measurement conditions. A software-based solution is also feasible, where the measurement system dynamically adjusts the hold time at each point based on the detection of high gradients. The results of the covered thermopile (see Figure 2 (right)) are shown in Figure 5. Although the results are similar to those of the uncovered sensor, deviations can be highlighted by calculating the difference between the two results, as illustrated in Figure 6. Significant deviations are observed in the edge regions of the LGT, which arise due to the different illuminated sensor areas. The larger area of the uncovered sensor results in greater averaging, leading to smoother transitions at the tunnel edges. In contrast, the covered sensor, with its smaller sensing area, is more effective at detecting local minima and maxima, thereby providing better sharpness in the tunnel's edge regions. This is evident when comparing Figure 4 (left) with Figure 5 (left). While the sensor with the larger surface area shows the plateau as flat and uniform, the sensor with the smaller surface area reveals inhomogeneities in the upper half of the plateau.

3.3 Transient Response

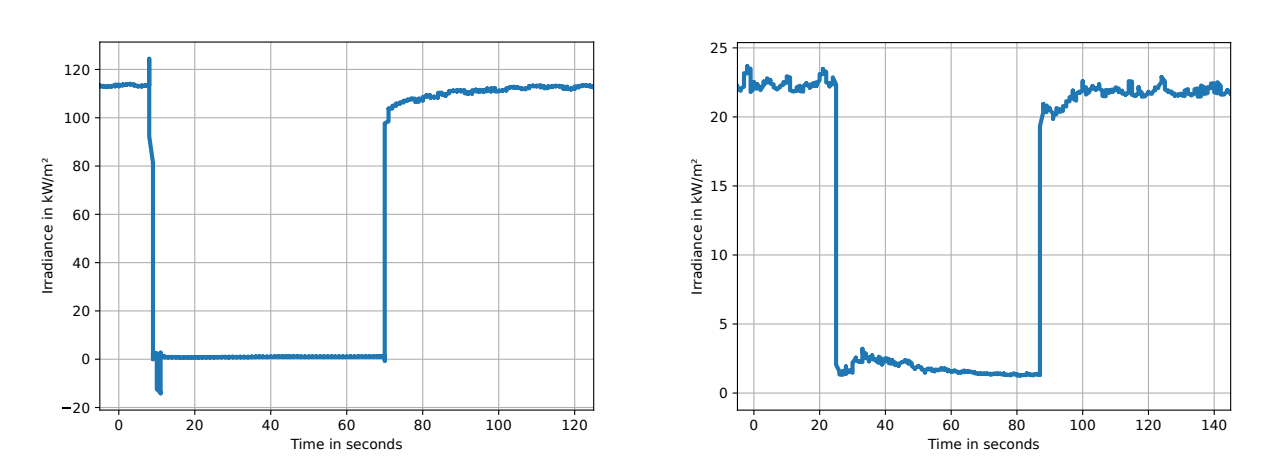


Figure 7. Time response of the uncovered (left) and covered (right) thermopile sensor. Note for the (right) Y-axis values: The sensor is not recalibrated. The absolute values are not correct due to the partial shading of the sensor.

Due to their operating principle, which is based on heat absorption, thermopiles inherently exhibit a certain degree of inertia. This inertia, or transient response, significantly affects the duration of a measurement process. For example, the focal

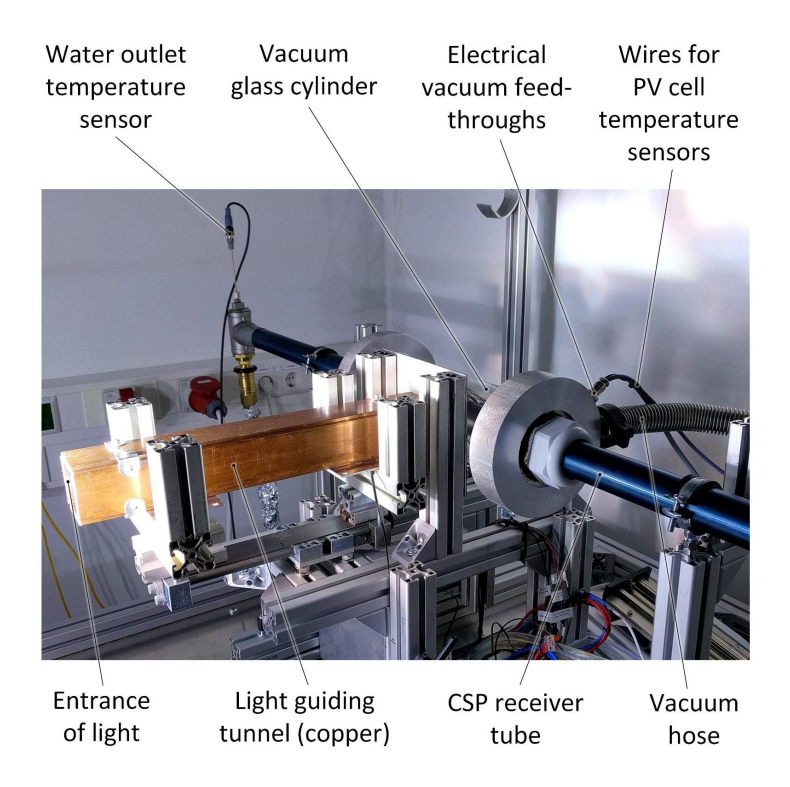


Figure 8. An example of the solar simulator for CSP applications: Absorber tube with CPV cells and vacuum glass cylinder of a parabolic trough system under test. [3]

point measurements required 27 minutes, the LGT measurements at low resolution took 37 minutes (1482 measurement points), and the high-resolution edge measurements took 53 minutes (2346 measurement points). This is because, at each measurement point, a certain amount of time must be waited for the sensor signal to stabilize. To better analyze this transient response, a measurement was conducted in which the sensor, in both uncovered and covered states, was abruptly shaded with an aluminum plate and then re-illuminated, while keeping the irradiance level constant. The results are shown in Figure 7. According to the thermopile datasheet [4], the response time is $0.2\,\mathrm{s}$ (63 %). Therefore, after $1\,\mathrm{s}$ (5 τ), the thermopile should be $99.3\,\%$ stabilized. This is only partially consistent with the measured results, as there is an initial rapid change in the output signal, but the final $\approx\!10\,\%$ takes several tens of seconds to stabilize. This behavior is also observed with the covered sensor area, where the stainless steel housing is shielded. There is no significant difference between the covered and uncovered sensor in terms of the general trend. The only noticeable difference is that the light fluctuations are more visible with the covered sensor, as the absolute values of the changes are smaller.

4. Conclusion

Despite the discrepancies in the sensor's timing response, it was demonstrated that a thermopile mounted on an XY table can be used to measure high-resolution irradiance distributions. The measurement time primarily depends on two factors: (a) the chosen resolution and (b) the thermopile's stabilization time. Measurement durations in the order of one hour impose strict requirements for maintaining consistent irradiation (e.g., from lamps) throughout this period. While changes can be partially compensated, this presents significant challenges [2]. Furthermore, the uncertainty of the sensor should be examined in more detail, which could not be accomplished due to the page limit of this format. However, it is expected that a measurement based on a thermopile

should be significantly more accurate than, for example, that of a CCD camera [2]. Overall, repeated measurements showed good stability and repeatability. Finally, Figure 8 illustrates an example application of the solar simulator with a light-guiding tunnel for characterizing CSP components of a parabolic trough system.

Data availability statement

The raw data of the measurement results can be requested from the corresponding author.

Underlying and related material

See [3] for a more detailed description of the solar simulator used in this work.

Author contributions

Conceptualization: R.F.; Data curation: R.F.; Funding acquisition: A.B., H.W.; Investigation: R.F., B.G.; Methodology: R.F.; Software: R.F.; Resources: R.F., A.B., B.G., H.W.; Supervision: H.W.; Validation: R.F.; Visualization: R.F.; Writing – original draft: R.F.; Writing – review and editing: R.F., B.G., H.W.

Competing interests

The authors declare that they have no competing interests.

Funding

This research was funded by the Austrian Research Promotion Agency (grant number 865065) with the Energy Research Programme, 4th Call.

References

- [1] A. Gallo, A. Marzo, E. Fuentealba, and E. Alonso, "High flux solar simulators for concentrated solar thermal research: A review", *Renewable and Sustainable Energy Reviews*, vol. 77, pp. 1385–1402, 2017, ISSN: 1364-0321. DOI: https://doi.org/10.1016/j.rser.2017.01.056.
- [2] J. Garrido, L. Aichmayer, W. Wang, and B. Laumert, "Characterization of the kth high-flux solar simulator combining three measurement methods", *Energy*, vol. 141, pp. 2091–2099, 2017, ISSN: 0360-5442. DOI: https://doi.org/10.1016/j.energy.2017.11.067.
- [3] A. Buchroithner, B. Gerl, R. Felsberger, and H. Wegleiter, "Design and operation of a versatile, low-cost, high-flux solar simulator for automated cpv cell and module testing", *Solar Energy*, vol. 228, pp. 387–404, 2021, ISSN: 0038-092X. DOI: https://doi.org/10.1016/j.solener.2021.08.068.
- [4] Hukseflux. "User manual sbg series", Accessed: Aug. 30, 2024. [Online]. Available: https://www.hukseflux.com/uploads/product-documents/SBG_series_manual_v2303_0.pdf.